Impact of carrier localization on the photoluminescence characteristics of (Ga,In)(N,As) and (Ga,In)(N,As,Sb) quantum wells

Fumitaro Ishikawa[a), b)], Álvaro Guzmán, Oliver Brandt, Achim Trampert, and Klaus H. Ploog
Paul-Drude-Institut für Festkörperelektronik, Hausvogteiplatz 5–7, 10117 Berlin, Germany
(Dated: October 28, 2008)

Using photoluminescence spectroscopy (PL), we carry out a comparative study of the optical properties of (Ga,In)(N,As) and (Ga,In)(N,As,Sb) quantum wells (QWs). The incorporation of Sb into (Ga,In)(N,As) results in a reduced quantum efficiency at low temperatures, but an improved one at room temperature (RT). A PL lineshape analysis as well as the temperature dependence of the PL peak energy reveals the existence of band-tail localized states in both material systems. The carrier localization energy is larger for (Ga,In)(N,As,Sb) than for (Ga,In)(N,As), leading to a longer radiative lifetime and thus a reduced quantum efficiency at low temperatures for the former material. The thermal quenching of the quantum efficiency is analyzed by a rate equation model, which shows that the density of non-radiative centers is reduced in (Ga,In)(N,As,Sb) resulting in an enhanced quantum efficiency at RT.

PACS numbers: 73.21.Fg,81.07.St,81.15.Hi

I. INTRODUCTION

Over the past decade, the material system (Ga,In)(N,As) has been of increasing physical and technological interest due to its potential use for low-cost and high-performance 1.3 and 1.55 μm telecommunication lasers on GaAs substrates.[1,2] The incorporation of a few percent of N into the host (In,Ga)As matrix induces a resonant nitrogen level, which splits the conduction band into two subbands and thus leads to an anomalous reduction of the band gap.[3] For emission at the long telecommunication wavelengths, the incorporation of large amounts of In and N is required. However, this enhances the phase separation tendency stemming from the inherent miscibility gap of (Ga,In)(N,As), resulting in strong composition modulations of the alloys.[4–6] To overcome these difficulties, a surfactant-mediated growth using Sb has been suggested as a possible solution.[7] Moreover, the incorporation of Sb extends the emission wavelengths towards longer wavelengths.[8] Recently, (Ga,In)(N,As,Sb) QWs were utilized for the successful achievements of room temperature (RT) continuous-wave operating lasers emitting at 1.55 μm.[9,10] The critical issue for the realization of these lasers is the improvement of the PL efficiency at RT.

The above mentioned composition modulations induce potential fluctuations in the band edge,[11,12] resulting in strong carrier localization which significantly affect the PL characteristics.[13–20] Up to now, however, there is only a limited number of studies concerning the impact of the incorporation of Sb on the PL characteristics of (Ga,In)(N,As) QWs.[21,22] In this article, we perform a comparative study of the PL characteristics of (Ga,In)(N,As) and (Ga,In)(N,As,Sb) QWs. We show that both carrier localization and nonradiatiove processes are modified upon the incorporation of Sb, resulting in a higher quantum efficiency of (Ga,In)(N,As,Sb) at RT.

II. EXPERIMENTAL

All the investigated samples were undoped and were grown on semi-insulating GaAs(001) substrates by plasma-assisted solid-source molecular beam epitaxy. A radio-frequency plasma source was used for the supply of active N. Prior to the growth of the structure, a 250 nm thick undoped GaAs buffer layer was grown at 580°C. We studied two sets of samples all of which contain a three-period multiple quantum well with 6.5 nm QWs sandwiched by 12 nm Ga(N,As) barriers. The first set contains (Ga,In)(N,As) QWs, while the second consists of (Ga,In)(N,As,Sb) QWs. These QWs were grown under identical conditions, except for the addition of Sb for the second set with an Sb_4 beam equivalent pressure (BEP) of 1.7×10^{-8} Torr. The growth was completed with a 36 nm GaAs cap layer. The structures were grown at a constant substrate temperature of 420°C. The growth rate for the QWs was 0.3 μm/h, and the As_4/(group III) BEP ratio was kept at 45.

In the following, we focus on two samples the composition of which was determined by high-resolution X-ray diffraction and secondary ion mass spectrometry. The contents of In and N in the QWs of sample #1 were thereby obtained to be 34% and 3.1%, respectively. Assuming an identical In and N content for sample #2, we can estimate an Sb content of about 3% in the QWs of sample #2. The Ga(N,As) barriers contain about 0.5% N for both samples. The composition of these QWs is summarized in Tab. I. Structurally, the samples are equivalent. In transmission electron micrographs (not shown here), the QWs appear compositionally perfectly homogeneous, and the interfaces are abrupt and flat.[23] The carrier localization discussed in this paper is thus not the result of phase separation or three-dimensional growth, but an inevitable consequence of the statistical disorder inherent for quaternary and pentanary alloys.

The optical properties of the samples was investigated by PL. The 633 nm line of a He-Ne laser was used for excitation. The signal was dispersed by a 0.22 m grating monochroma-

a) Electronic mail: ishikawa@eei.eng.osaka-u.ac.jp
b) Present address: Graduate School of Engineering, Osaka University, Yamadaoka 2-1, Suita, Osaka, 565-0871 Japan.

tor and detected by a liquid-nitrogen-cooled Ge photodiode connected to a standard lock-in amplifier. Prior to the measurements, rapid thermal annealing at 750°C for 60 s was employed to enhance the luminescence yield.[8,24] The measurements were typically carried out with an excitation density P_{ex} of 4 W/cm^2 unless otherwise mentioned.

III. PL INTENSITY AT 290 K AND 15 K

Figure 1 (a) displays the PL spectra of samples #1 and #2 measured at 290 K. The incorporation of Sb improves the PL intensity and leads to a redshift of the peak position from 0.914 eV to 0.874 eV. In Figs. 1 (b) and (c), the PL intensities measured at 290 and 15 K, respectively, are plotted for the two sets of (Ga,In)(N,As) and (Ga,In)(N,As,Sb) QWs. The samples were grown under identical conditions except for the As flux. As seen in Fig. 1 (b), the incorporation of Sb generally improves the PL intensity at 290 K as has been reported in this system.[7–10,21,22] In contrast, all the (Ga,In)(N,As,Sb) QWs have lower PL intensities than the (Ga,In)(N,As) QWs at 15 K, as seen in Fig. 1 (c). The impact of Sb incorporation on the optical properties of (Ga,In)(N,As) QWs is thus more complex than assumed previously.[7,8,21,22] In the following, we attempt to clarify this behavior by a detailed examination of the PL lineshape and the temperature dependence of both the PL peak energy and efficiency.

IV. PL SPECTRA AT LOW TEMPERATURE

Figures 2 (a) and (b) display PL spectra at 15 K for samples #1 and #2, respectively. The measurements were taken with different excitation intensities P_{ex} as indicated in the figures. For both samples, we observe a blueshift and narrowing in linewidth with increasing excitation density. This behavior is a signature for the existence of localized states and their increasing occupation by bound excitons. With increasing excitation density, the localized states are saturated, causing a blueshift and a spectral narrowing.[25,26] As clearly seen in the figures, the former of these phenomena is more evident for sample #2 when compared to sample #1. By increasing P_{ex} from 0.04 to 4 W/cm^2, the spectra of sample #1 basically remain their spectral position at 961 meV, while their full width at half maximum (FWHM) is reduced from 20 meV to 18 meV. In contrast, the spectra of sample #2 exhibit a significant peak shift from 911 meV to 920 meV. Their FWHM remains almost constant, but the low energy tail is suppressed with increasing P_{ex}.

For a quantitative understanding of these excitation-density dependent changes, we perform a lineshape analysis for spectra measured at the lowest P_{ex}, for which the influence of localized states is most prominent.[27] Figures 3 (a) and (b) show PL spectra for samples #1 and #2, respectively, measured at 15 K with P_{ex} of 0.04 W/cm^2. As seen in the figures, both samples exhibit asymmetric PL lineshapes with a pronounced low energy tail. The tail stems from the recombination from deep localized states as commonly observed in (Ga,In)(N,As)[14–16,20] as well as in other compound semiconductor alloys having potential fluctuations.[28]

We assume that the localized states possess an exponentially distributed density of states.[29] Then the lineshape at an energy E can be expressed as[30]

$$I_{PL}(E) = \int_{-\infty}^{E_{\max}} I_0 \exp\left[-\frac{(E-E_0)^2}{2\sigma_0^2}\right] N_0 \exp(-\delta E_0) dE_0, \quad (1)$$

with the density-of-state distribution $N_0 \exp(-\delta E_0)$ and a Gaussian lineshape $I_0 \exp[-((E-E_0)^2)/2\sigma_0^2]$ associated with each level of the distribution. N_0 and I_0 are energy independent constants. At a certain generation rate, all the levels up to $E = E_{max}$ are filled by excitons. As the spectra are normalized to their maximum, the fits involve free parameters, namely, E_{max}, σ_0 and δ.

The fits obtained are presented in Figs. 3 (a) and (b) as solid lines, and the fitting parameters are summarized in Tab. II. A good fit is obtained for sample #1 as shown in Fig. 3 (a), using $E_{max} = 0.966$ eV, $\sigma_0 = 5.4$ meV and $\delta = 95$ eV^{-1}. In contrast, the fit for sample #2 substantially deviates from the data at the low energy side, indicating that the density-of-state distribution is not well described by a simple exponential in this case. The parameters for the displayed curve in Fig. 3 (b) are $E_{max} = 0.918$ eV, $\sigma_0 = 6.0$ meV and $\delta = 60$ eV^{-1}. The localized states in sample #2 exhibit an energetically wider density-of-state distribution compared to those of sample #1.

The vertical bars in Figs. 3 (a) and (b) indicate the free-state transition energy deduced from the result of the temperature dependence of the PL peak energy, which will be discussed in the following section V. The larger deviation from the free-state energy to the spectral peak position confirms the wider density-of state-distribution for sample #2. Note that the free-state transition energy is in excellent agreement with E_{max} for sample #1, and only slightly higher in the case of sample #2.

The above results indicate that the incorporation of Sb during growth induces a deeper localization of carriers than present in (Ga,In)(N,As) QWs without Sb. A likely explanation for this finding is that Sb induces stronger fluctuations of the local potential simply due to the presence of In-Sb bonds. Furthermore, compositional disorder caused by the statistical distribution of the constituent atoms will be enhanced in a pentanary alloy compared to a quaternary one.[11] In any case, the radiative lifetime is known to be prolonged with increasing localization strength, i. e., depth of the localized level.[31] A different radiative lifetime may explain the different PL quantum efficiency at low temperatures of samples #1 and #2 as seen in Fig. 1 (c).

V. TEMPERATURE DEPENDENCE OF THE PL PEAK ENERGY

In the following, we discuss the temperature dependence of the PL peak energy, which has been frequently employed to examine exciton localization phenomena in this material system.[14,15,17,20]

Figure 4 shows the temperature dependence of the PL peak

energy for samples #1 and #2, measured at temperatures between 15 and 290 K with different P_{ex} as indicated in the figure. Measurements up to 290 K were only possible with the highest P_{ex}. The peak energies of both samples exhibit the so-called *S-shape* behavior. When the temperature increases from 15 to 40 K, the PL peak energy redshifts. However, a pronounced blueshift is observed from 40 to 100 K, and a further increase of the temperature above 100 K leads to a redshift again. This behavior occurs due to the competition between the transfer of localized carriers toward deeper lying localized states and their thermalization toward extended free states.[14,15,17,20] As observed in Sec. IV, the peak energy blueshifts with increasing P_{ex} for both samples #1 and #2 at temperatures lower than 40 K where the carrier thermalization is negligible. As explained above, this blueshift occurs due to the progressive filling of the band tail states.[14,20,25]

To estimate the transition energy from the free states, we fit the PL peak energy for data measured between 70 and 290 K with the highest P_{ex} of 4 W/cm^2. The transition energy at a temperature T can be expressed with Pässler's formula as[32]

$$E(T) = E(0) - \frac{\alpha\Theta}{2}\left[\sqrt[4]{1+\frac{\pi^2}{6}\left(\frac{2T}{\Theta}\right)^2+\left(\frac{2T}{\Theta}\right)^4}-1\right]. \quad (2)$$

Here Θ is the effective phonon temperature and α denotes the limiting slope such that $\alpha = -dE/dT|_{T\to\infty}$. The fit returns $E(0)$=0.969 eV, $\alpha = 3.6\times10^{-4}$ (eV·K^{-1}) and Θ=343 K for sample #1, and $E(0)$=0.930 eV, $\alpha = 5.3\times10^{-4}$ (eV·K^{-1}) and Θ=593 K for sample #2. All parameters are also listed in Table II.

The maximum energy deviation ΔE between the experimental PL peak energy and $E(T)$ determined from Eq. 2 represents the localization energy of carriers bound to the deeper lying localized states.[15] We obtain a ΔE of 11 and 28 meV for samples #1 and #2, respectively, as also listed in Table II. The larger localization energy obtained for sample #2 is consistent with the discussion at the end of Sec. V.

VI. TEMPERATURE DEPENDENCE OF THE QUANTUM EFFICIENCY

In the following, we perform a quantitative analysis of the temperature dependence of the quantum efficiency for samples #1 and #2 as shown in Fig. 5. These data are derived from the spectrally integrated PL intensity measured at P_{ex} of 4 W/cm^2. The absolute value for the quantum efficiency is estimated by comparing the integrated PL intensity of samples #1 and #2 to that of an (In,Ga)As QW with particularly intense emission, the quantum efficiency of which is assumed to be unity at low temperature. For both samples, the temperature dependence is characteristic for this materials system, in that a steep drop at intermediate temperatures is followed by a saturation at higher temperatures.[17,20,33,34] Rubel et al. concluded from Monte-Carlo simulations that this particular behavior is caused not only by the interplay between radiative and non-radiative recombination processes, but also by the interaction between excitons in localized and extended states.[33]

For a quantitative understanding of this behavior, we employ a simple rate equation model considering the radiative and nonradiative decay of both localized (n_b) and extended (n_x) states as well as their interaction.[26] We assume that the recombination dynamics is monomolecular in the entire temperature range, which is not necessarily correct but generally accepted at this low excitation density. The physical situation we are concerned with is schematically shown in Fig. 6, and is described by the following set of rate equations

$$dn_x/dt = G - \gamma_x n_x - \gamma_{xn} n_x - b_r n_x N_F + b_e n_b, \quad (3)$$

$$dn_b/dt = -\gamma_b n_b - \gamma_{bn} n_b + b_r n_x N_F - b_e n_b, \quad (4)$$

where G is the generation rate, $\gamma_x = \gamma_x^0/T$ and γ_b are radiative and γ_{xn} and γ_{bn} non-radiative recombination rates. The two other terms describe the capture (b_r) and release (b_e) of localized excitons. N_F denotes the density of unoccupied localized states with a total density $N_L = N_F + n_b$ of localized states.

The above model allows, in principle, an excellent fit of the data displayed in Fig. 5. There are, however, too many free parameter, and the fit is not unique. For simplifying the problem under consideration, we first of all follow the method outlined in Ref. 26. This approach reduces the problem to one where essentially only the ratios γ_b/γ_{bn}, γ_x/γ_{xn}, and $b_r/b_e \propto \exp(E_b/kT)$ with the binding energy E_b determine the temperature dependence of the quantum efficiency. Note that E_b represents a mean localization energy for excitons, while ΔE introduced above reflects the maximum localization energy within the diffusion length of the excitons. Second, in the limit of $T \to 0$ the population of free excitons is essentially zero, and the quantum efficiency at low temperatures is simply given by

$$\eta_{LT} \approx \gamma_b/\gamma_{bn}. \quad (5)$$

From the experimental result shown in Fig. 5, η_{LT} is 3.7×10^{-2} for sample #1 and 1.5×10^{-2} for sample #2. As described in Sec. IV, we attribute the difference of the quantum efficiency between samples #1 and #2 at low temperatures to the different radiative lifetimes.[31] If we, for the sake of getting absolute values, assign a value of 1×10^{14} cm^{-2}ns^{-1} to $\gamma_{nb}N_L$ for both samples, the fits depicted in Fig. 5 return the following parameters: $E_b = 21$ meV, $\gamma_x^0 = 8.9$ ns^{-1}K and $\gamma_{xn} = 8.0\times10^4$ ns^{-1} for sample #1, and $E_b = 9$ meV, $\gamma_x^0 = 9.8$ ns^{-1}K, $\gamma_{xn} = 6.5\times10^3$ ns^{-1} for sample #2.

The values obtained for E_b seem contradictory to the results in Secs. IV and V, and in particular to the values for ΔE which clearly imply a stronger localization for sample #2. However, upon a closer inspection of the fits depicted in Fig. 5, it becomes clear that our simplified model is not able to describe the convex shape of the data observed for sample #1. As a result, the fit algorithm artificially increases the value of E_b which determines the onset of the decrease of the quantum efficiency. The high value of E_b for sample #1 is just nothing but an artifact. The values for γ_x^0 are, as one would expect, almost identical, and are comparable to those reported for other III-V semiconductor QWs.[35,36] In contrast, the values obtained for γ_{xn} are different by more than one order of magnitude, directly reflecting the strength of the thermal quenching in quantum

efficiency for the two different samples. As proposed previously, this difference is most likely due to a reduction of the concentration of point defects by the surfactant effect of Sb.[37,38]

VII. SUMMARY AND CONCLUSIONS

We have carried out a comparative study of the photoluminescence characteristics of (Ga,In)(N,As) and (Ga,In)(N,As,Sb) QWs. The incorporation of Sb degrades the PL efficiency at low, but improves it at high temperatures. A PL lineshape analysis as well as the temperature dependence of the PL peak energy reveals the existence of localized states in both materials systems. The carrier localization energy is larger for (Ga,In)(N,As,Sb) than for (Ga,In)(N,As), leading to a longer radiative lifetime and thus a reduced quantum efficiency at low temperatures for the former material. The thermal quenching of the quantum efficiency is analyzed by a rate equation model, which shows that the non-radiative recombination rate is reduced in (Ga,In)(N,As,Sb) resulting in an enhanced quantum efficiency at RT. We believe that this difference is most likely due to a reduction of the concentration point defects by the surfactant effect of Sb.

Acknowledgments

The authors are indebted to E. Luna for fruitful discussions and to K. Hagenstein, H.-P. Schönherr and G. Paris for their invaluable technical assistance.

[1] M. Kondow, K. Uomi, A. Niwa, T. Kitatani, S. Watahiki, and Y. Yazawa, Jpn. J. Appl. Phys. **35**, 1273 (1996).

[2] G. Jaschke, R. Averbeck, L. Geelhaar, and H. Riechert, J. Cryst. Growth **278**, 224 (2005).

[3] W. Shan, W. Walukiewicz, J. W. Ager III, E. E. Haller, J. F. Geisz, D. J. Friedman, J. M. Olson, and S. R. Kurtz, Phys. Rev. Lett. **82**, 1221 (1999).

[4] I. Ho and G. B. Stringfellow, J. Crys. Growth **178**, 1 (1997).

[5] J. Neugebauer and C. G. Van de Walle, Phys. Rev. B **51**, 10568 (1995).

[6] A. Trampert, J.-M. Chauveau, K. H. Ploog, E. Tournié, and A. Guzmán, J. Vac. Sci. Technol. B **22**, 2195 (2004).

[7] X. Yang, M. J. Jurkovic, J. B. Heroux, and W. I. Wang, Appl. Phys. Lett. **75**, 178 (1999).

[8] J. S. Harris Jr., J. Crys. Growth **278**, 3 (2005).

[9] J. A. Gupta, P. J. Barrios, J. A. Caballero, D. Poitras, G. C. Aers, G. Pakulski, and X. Wu, Appl. Phys. Lett. **89**, 151119 (2006).

[10] Z. C. Niu, S. Y. Zhang, H. Q. Ni, D. H. Wu, H. Zhao, H. L. Peng, Y. Q. Xu, S. Y. Li, Z. H. He, Z. W. Ren, et al., Appl. Phys. Lett. **87**, 231121 (2005).

[11] E. F. Schubert and K. Ploog, J. Phys. C: Solid State Phys **18**, 4549 (1985).

[12] J. W. Harrison and J. R. Hauser, Phys. Rev. B **13**, 5347 (1976).

[13] I. A. Buyanova, W. M. Chen, and B. Monemar, MRS Internet J. Nitride Semicond. Res. **6**, 2 (2001).

[14] I. A. Buyanova, W. M. Chena, and C. W. Tu, Solid-State Electron. **47**, 467 (2003).

[15] M.-A. Pinault and E. Tournie, Appl. Phys. Lett. **78**, 1562 (2001).

[16] A. Polimeni, M. Capizzi, M. Geddo, M. Fischer, M. Reinhardt, and A. Forchel, Appl. Phys. Lett. **77**, 2870 (2000).

[17] L. Grenouillet, C. Bru-Chevallier, G. Guillot, P. Gilet, P. Duvaut, C. Vannuffel, A. Million, and A. Chenevas-Paule, Appl. Phys. Lett. **76**, 2241 (2000).

[18] A. Kaschner, T. Lüttgert, H. Born, A. Hoffmann, A. Y. Egorov, and H. Riechert, Appl. Phys. Lett. **78**, 1391 (2001).

[19] T. K. Ng, S. F. Yoon, W. J. Fan, W. K. Loke, S. Z. Wang, and S. T. Ng, J. Vac. Sci. Technol. B **21**, 2324 (2003).

[20] H. D. Sun, M. Hetterich, M. D. Dawson, A. Y. Egorov, D. Bernklau, and H. Riechert, J. Appl. Phys. **92**, 1380 (2002).

[21] S. R. Bank, M. A. Wistey, H. B. Yuen, V. Lordi, V. F. Gambin, and J. J. S. Harris, J. Vac. Sci. Technol. B **23**, 1320 (2005).

[22] H. D. Sun, S. Calvez, M. D. Dawson, J. A. Gupta, G. I. Sproule, X. Wu, and Z. R. Wasilewski, Appl. Phys. Lett. **87**, 181908 (2005).

[23] Á. Guzmán, E. Luna, F. Ishikawa, and A. Trampert, Submitted to J. Cryst. Growth: Special issue for the 15th International Conference on Molecular Beam Epitaxy (MBE 2008).

[24] S. G. Spruytte, C. W. Coldren, J. S. Harris, W. Wampler, P. Krispin, K. H. Ploog, and M. C. Larson, J. Appl. Phys. **89**, 4401 (2001).

[25] P. G. Eliseev, P. Perlin, J. Lee, and M. Osiński, Appl. Phys. Lett. **71**, 569 (1997).

[26] O. Brandt, P. Waltereit, S. Dhar, U. Jahn, Y. J. Sun, A. Trampert, K. H. Ploog, M. A. Tagliente, and L. Tapfer, J. Vac. Sci. Technol. B **20**, 1626 (2002).

[27] D. Ouadjaout and Y. Marfaing, Phys. Rev. B **46**, 7908 (1992).

[28] D. Ouadjaout and Y. Marfaing, Phys. Rev. B **41**, 12096 (1990).

[29] M. Oueslati, C. Benoit, and M. Zouaghi, Phys. Rev. B **37**, 3037 (1988).

[30] U. Jahn, S. Dhar, R. Hey, O. Brandt, J. Miguel-Sánchez, and Á. Guzmán, Phys. Rev. B **73**, 125303 (2006).

[31] E. I. Rashba and G. E. Gurgenishvili, Sov. Phys.- Solid State **4**, 759 (1962).

[32] R. Päsller, Phys. Stat. Sol. (b) **200**, 155 (1997).

[33] O. Rubel, S. D. Baranovskii, K. Hantke, B. Kunert, W. W. Rühle, P. Thomas, K. Volz, and W. Stolz, Phys. Rev. B **73**, 233201 (2006).

[34] M. Bissiri, V. Gaspari, A. Polimeni, G. B. H. von Högersthal, M. Capizzi, A. Frova, M. Fischer, M. Reinhardt, and A. Forchel, Appl. Phys. Lett. **79**, 2585 (2001).

[35] J. Feldmann, G. Peter, E. O. Göbel, P. Dawson, K. Moore, C. Foxon, and R. J. Elliott, Phys. Rev. Lett. **59**, 2337 (1987).

[36] J. Martinez-Pastor, A. Vinattieri, L. Carraresi, M. Colocci, P. Roussignol, and G. Weimann, Phys. Rev. B **47**, 10456 (1993).

[37] C. E. C. Wood, T. M. Kerr, T. D. McLean, D. I. Westwood, J. D. Medland, S. Blight, and R. Davies, J. Appl. Phys. **60**, 1300 (1986).

[38] Y. G. Sadofyev, S. R. Johnson, S. A. Chaparro, Y. Cao, D. Ding, J.-B. Wang, K. Franzreb, and Y.-H. Zhang, Appl. Phys. Lett. **84**, 3546 (2004).

Tables

TABLE I: Composition of the two samples under investigation. Listed are the sample numbers, materials, and concentrations of In, N, and Sb within the QWs. The Ga(N,As) barriers contain about 0.5% N in both samples.

Sample	Material	In (%)	N (%)	Sb (%)
#1	(Ga,In)(N,As)	34	3.1	—
#2	(Ga,In)(N,As,Sb)	34	3.1	≈3

TABLE II: Parameters E_{max}, σ_0 and δ obtained from the fit of the PL lineshape shown in Fig. 3 as well as $E(0)$, α and Θ obtained from the fit of the PL peak energy shown in Fig. 4. The largest energy deviation ΔE between the fit and the experimental data is also shown.

	E_{max}	σ_0	δ	$E(0)$	α	Θ	ΔE
Sample	(eV)	(meV)	(eV^{-1})	(eV)	($eV \cdot K^{-1}$)	(K)	(meV)
#1	0.966	5.4	95	0.969	3.6×10^{-4}	343	11
#2	0.918	6.0	60	0.930	5.3×10^{-4}	593	28

Figures

FIG. 1: (a) PL spectra of samples #1 and #2 measured at 290 K. Plot of PL intensities at 290 (b) and 15 K (c) for the two sets of (Ga,In)(N,As) (■) and (Ga,In)(N,As,Sb) QWs (□) grown at different As_4/(group III) BEP ratio. The data points corresponding to samples #1 and #2 are highlighted.

FIG. 2: PL spectra for samples #1 (a) and #2 (b) measured at different excitation density P_{ex} at 15 K.

FIG. 3: PL spectra for samples #1 (a) and #2 (b) measured at 15 K and P_{ex} of 0.04 W/cm^2. The open circles are experimental data and the solid lines are the fit using Eq. 1. The vertical bars indicate the free-state transition energy deduced from the fit shown with a solid line in Fig. 4.

FIG. 4: Temperature dependence of the PL peak energy measured at different P_{ex} as indicated in the figure. The solid lines are fits using Eq. 2.

FIG. 5: Temperature dependence of the quantum efficiency for samples #1 and #2. The symbols are experimental data obtained from the integrated PL intensity.

FIG. 6: Schematics of the coupling between and recombination from localized and free states.

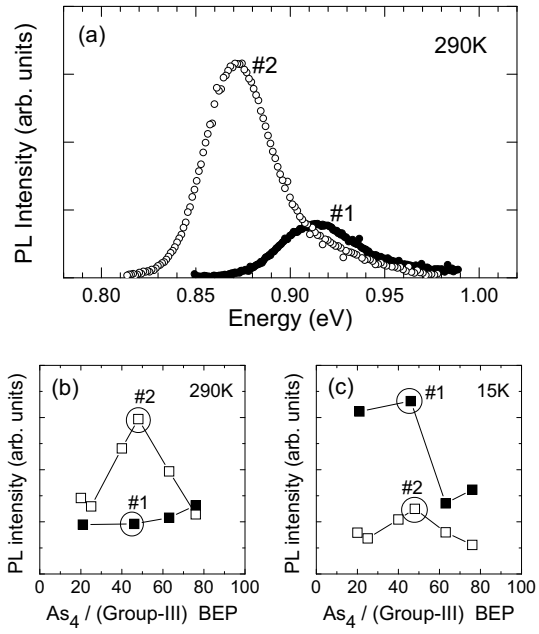

FIG. 1: F. Ishikawa et al.

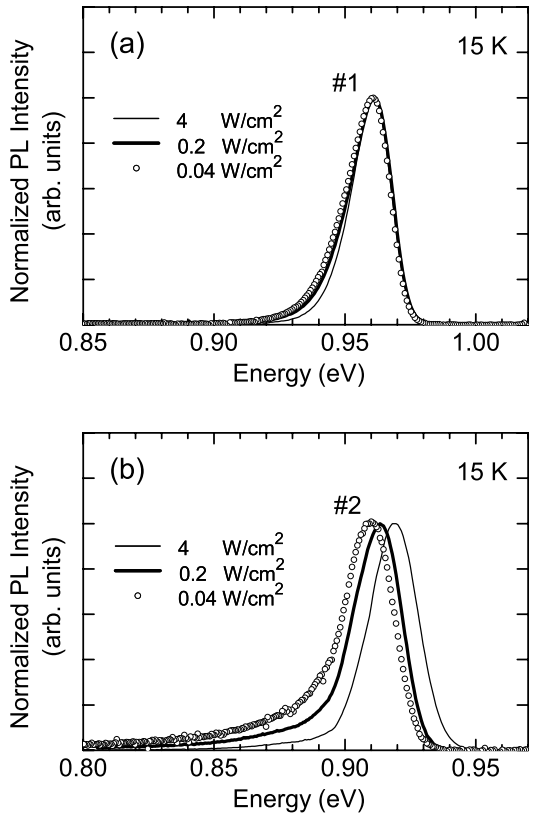

FIG. 2: F. Ishikawa et al.

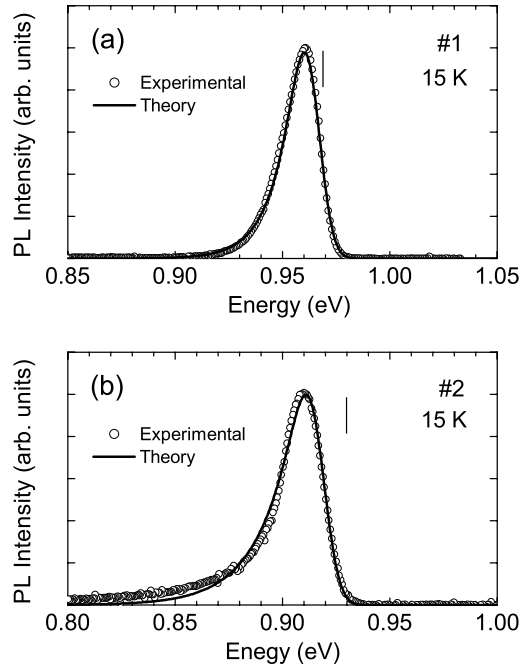

FIG. 3: F. Ishikawa et al.

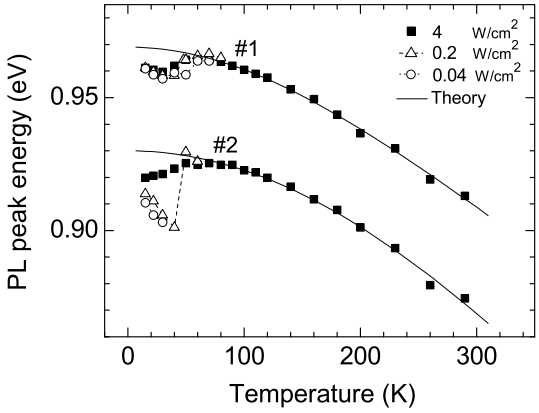

FIG. 4: F. Ishikawa et al.

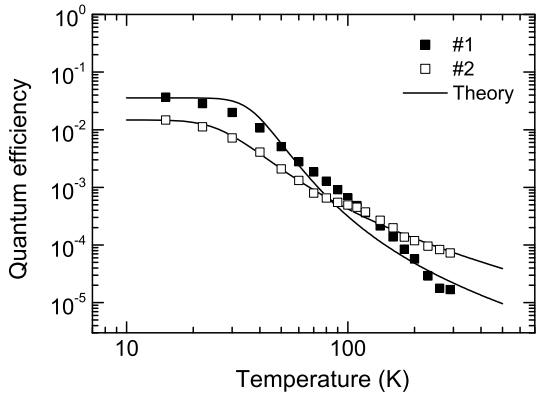

FIG. 5: F. Ishikawa et al.

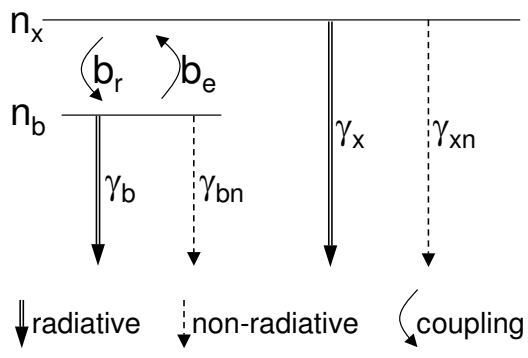

FIG. 6: F. Ishikawa et al.